Thickness Dependence of Plasmonic Charge Carrier Generation in Ultrathin a-Si:H Layers for Solar Cells

ARTICLE *in* ACS NANO · AUGUST 2011

Impact Factor: 12.88 · DOI: 10.1021/nn201074z · Source: PubMed

3 AUTHORS:

Viktoria Gusak
Chalmers University of Technology
10 PUBLICATIONS **74** CITATIONS
SEE PROFILE

Bengt Herbert Kasemo
Chalmers University of Technology
497 PUBLICATIONS **23,202** CITATIONS
SEE PROFILE

Carl Hägglund
Uppsala University
37 PUBLICATIONS **923** CITATIONS
SEE PROFILE

Thickness Dependence of Plasmonic Charge Carrier Generation in Ultrathin a-Si:H Layers for Solar Cells

Viktoria Gusak, Bengt Kasemo, and Carl Hägglund*

Department of Applied Physics, Chalmers University of Technology, SE-412 96 Göteborg, Sweden

ABSTRACT Nanocomposite layers of Ag nanoparticles and a-Si:H film constitute attractive candidates for the realization of ultrathin "two-dimensional" plasmonic solar cells, with an ideal 18% efficiency predicted for an average layer thickness of only 20 nm. By combining optical spectroscopy with photoconductivity measurements, we here characterize different contributions to the light absorption and charge carrier generation in such nanocomposites. We focus in particular on the important role of the absorber layer thickness for these processes, by studying a range of a-Si:H thicknesses from 9 to 67 nm. Through detailed comparison with numerical calculations by the finite element method, observed experimental features are connected to specific resonance modes and charge carrier generation mechanisms. The influence of dipolar and quadrupolar near-field distributions are evaluated with respect to different figures of merit for plasmonic solar cells. We briefly discuss how the present findings may be implemented in practical solar cell configurations.

KEYWORDS: ultrathin plasmonic solar cells · nanocomposites · 2D photovoltaics · amorphous hydrogenated silicon · figure of merit

The experimental conversion efficiency of around 10% attained, so far, for hydrogenated amorphous silicon (a-Si:H) thin film solar cells,[1] is much lower than the theoretical Shockley–Queisser detailed balance limit[2] of about 27% for the a-Si:H optical band gap of 1.7 eV.[3] This difference arises primarily from an inherently high density of tail and defect states in the a-Si:H band gap, which in turn leads to recombination losses, curtailed carrier transport, and lowering of the open circuit voltage.[4] The problem is more severe in *doped* a-Si:H due to its even higher concentration of recombination centers. In solar cell devices, this situation is normally handled through the use of p-i-n or n-i-p architectures comprising extremely thin (20–30 nm) p- and n-doped layers and a thicker (up to 1000 nm) intrinsic region where most of the light absorption takes place.[4,5] The layer thickness of the device is a compromise between the requirements to maximize optical absorption (benefitting from thicker films) and minimizing recombination and transport losses (benefitting from thinner films), respectively.

Nanoparticle plasmons offer an opportunity to improve this situation, as they allow for the use of much thinner layers with comparably small losses of optical absorption. For instance, recent theoretical work suggests an ideal conversion efficiency of 18% for a combined Ag/a-Si:H nanocomposite layer thickness of only 20 nm when backed up by a reflective support.[6] Thanks to the shorter carrier collection lengths in such ultrathin absorber layers, recombination and transport losses may be suppressed, and an ideal efficiency may be easier to approach. For instance, the effect of Staebler–Wronski degradation of a-Si:H has been observed to be reduced in thinner films.[7] There is even some experimental support for the possibility to go beyond the Shockley–Queisser limit by exploitation of ballistic (hot) carrier transport in such thin films.[8,9]

Plasmonic solar cells combining metal nanoparticles with a-Si:H have attracted increasing attention during the past few years.[10–16] Most work has focused on the exploitation of *far-field* effects induced by light scattering of the plasmonic nanoparticles. The resulting increase of optical path length leads to enhanced light absorption in the a-Si:H layer.[11–14,16] For this approach, the nanoparticles are typically located at the front or rear of the a-Si:H film with a transparent conductive oxide spacer/contact layer separating the metal nanoparticles from the a-Si:H. Nanoparticles of Al, Au, and Ag have been explored, among which Ag has the highest quality factor[17] over the relevant wavelength range and therefore the smallest internal dissipation losses. Results have primarily been evaluated in terms of photocurrent or absorption enhancement factors, calculated as ratios for samples with and without plasmonic particles. Typical a-Si:H film thicknesses in the range of 130 to 280 nm have been studied, with

* Address correspondence to carl.hagglund@chalmers.se.

Received for review March 22, 2011 and accepted July 6, 2011.

Published online July 06, 2011
10.1021/nn201074z

wavelength integrated enhancement factors of up to about 1.5 demonstrated.

Plasmon *near-field* induced light absorption begins to dominate over far-field effects below a length scale given by $(\lambda/n)/2\pi$, where λ/n is the wavelength in the nanostructured semiconductor with n being its (effective) refractive index. This less explored absorption and enhancement route has its physical origin in the locally amplified, nonpropagating part of the "scattered" electric field. Moulin *et al.*[10] studied the influence of a Ag metal island film on the performance of an ultrathin a-Si:H solar cell with an a-Si:H thickness of 40 nm. They found a substantial increase of the quantum efficiency in the presence of Ag nanoparticles for wavelengths exceeding the optical band gap threshold and attributed this effect to either photoemission of hot electrons from the metal nanoparticles, as a result of plasmon decay to electron–hole pairs within the nanoparticle, or to a near-field effect coupled to states at the metal/semiconductor interface.[10]

In the present work, we study the experimentally measured optical and opto-electronic properties of quasi-random, nanofabricated Ag nanoparticle distributions (Figure 1d–g), covered by ultrathin a-Si:H layers (Figure 1a) with thicknesses t in the range of 9 to 67 nm. We investigate the dependence on a-Si:H thickness in detail, as this is a key parameter to optimize for (plasmonic) solar cells.[18] Although the influence of spacers between plasmonic nanoparticles and ultrathin absorbing material has been studied to some extent,[19] surprisingly few works address the role of the absorber layer thickness itself. The thinnest composites considered here are well within the near-field dominated regime according to the criterium given above, whereas the thicker films give rise to significant finite size (retardation/interference) effects. Using calculations by the finite element method (FEM), we identify maxima associated with the different plasmon modes dominating for different thicknesses/wavelengths (see further Figure 1b,c). The results are analyzed in light of two alternative figures of merit used in the literature for quantifying the benefits of plasmonic components in solar cells.

RESULTS AND DISCUSSION

Plasmon-Enhanced Optical Absorption and Charge Carrier Generation in a-Si:H. Photoconductivity measurements were used to quantify Ag nanoparticle plasmonic contributions to the charge carrier generation rate in the a-Si:H layer. The a-Si:H layer provides a continuous conduction path between the probing electrodes, as illustrated in Figure 1a. Upon light absorption, free charge carriers are created in the a-Si:H layer and contribute to measurable conductivity, or potentially a photocurrent if in a solar cell configuration. The advantage of the simplified geometry used in this work is that the charge separation does not depend on built-in fields associated

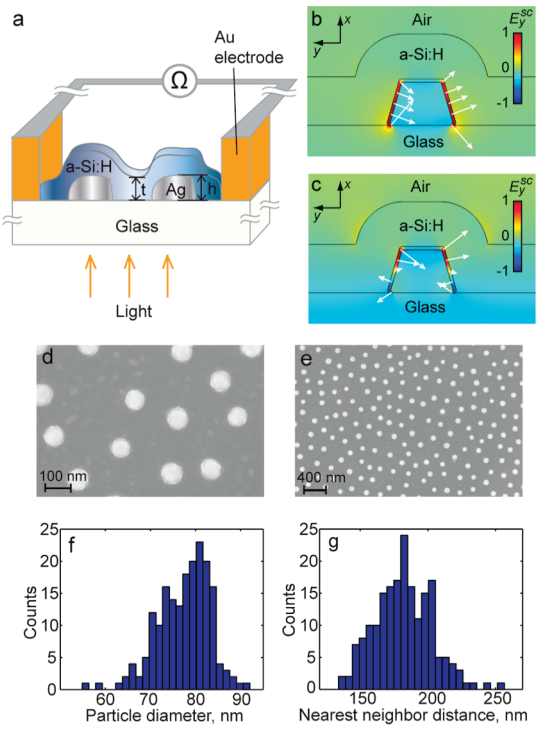

Figure 1. (a) Sample and electrode configuration used for the photoconductivity measurements. The sample consists of nanofabricated Ag nanoparticles of height *h* covered by an a-Si:H film of thickness *t*, in an area flanked by Au finger electrodes. In (b) and (c), calculations by the finite element method of the scattered electric field are presented. The a-Si:H thickness was 45 nm in both cases, and light is incident from the bottom along the *x*-axis, that is, perpendicular to the a-Si:H film plane. The wavelengths are 670 nm in (b) and 570 nm in (c). The scattered field components just outside the Ag particle surface are indicated by white arrows. In (b), at 670 nm wavelength, the response is of mainly dipolar character as seen by the fairly uniform direction of the scattered near-field. At the shorter 570 nm wavelength in (c), more of a quadrupolar character is demonstrated by the opposing scattered field vectors (mainly positive in *y* in the lower part and negative in the upper part of the a-Si:H/particle structure). The SEM images in (d) and (e) show typical quasi-random distributions of Ag disks used in this work. In all cases, the disks had a nominal diameter of 60 nm and height of 40 nm. The imaged samples are covered by a 9 nm a-Si:H layer. The histograms in (f) and (g) show typical distributions of particle diameters and nearest neighbor distances, respectively.

with a solar cell junction. The strength of a built-in field depends on the thicknesses of the doped and intrinsic regions of the device and leads to variations of the charge separation efficiency.[9] When the photoconductivity is probed laterally across the film by means of an external voltage instead, the situation remains more equivalent for different thicknesses of the a-Si:H film. We found that the measured photoconductivity had a linear dependence on photon flux (to within ±2%) throughout the range used (up to about 1.5 mW/cm^2), which is crucial for its validity as a measure of the charge carrier generation efficiency.

The photoconductance was measured as a function of wavelength both with and without Ag nanodisks as

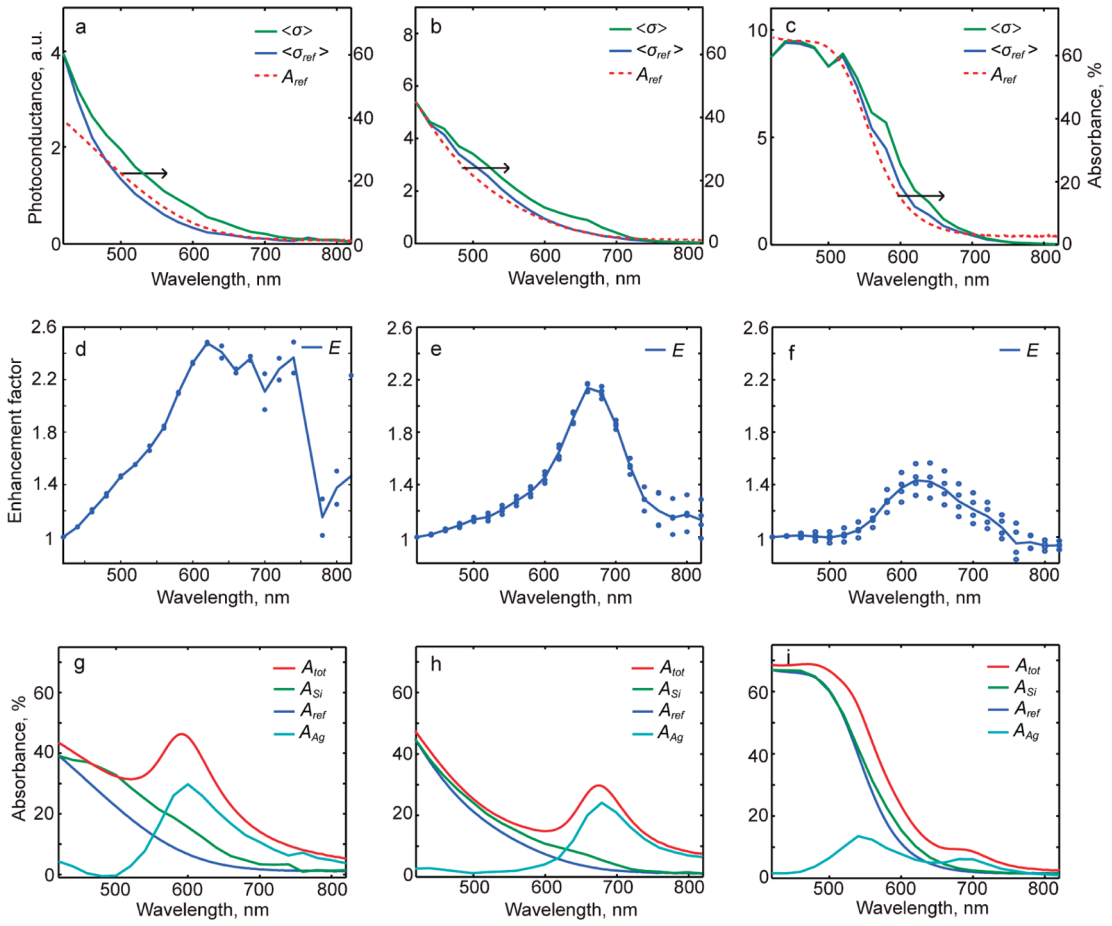

Figure 2. Thickness dependences illustrated by Ag particles covered by 12, 32, and 67 nm a-Si:H layers (left, middle, and right columns, respectively). The top figure row (a–c) shows an average of normalized photoconductance spectra ($\langle\sigma\rangle$ and $\langle\sigma_{ref}\rangle$) and the measured absorbance of the corresponding flat a-Si:H films (A_{ref}). The middle row (d–f) displays the photoconductivity enhancement associated with the plasmons. The points in panels (e) and (f) represent values of E obtained from combinations of photoconductances of two a-Si:H/Ag and two reference samples, which led to four values of the enhancement factor at each wavelength measured. For the 12 nm film from panel (d), two a-Si:H/Ag and one reference sample were measured, which led to two values of E at each wavelength. The bottom row (g–i) shows the photoconductance derived estimates A_{Si} and A_{Ag} of the different contributions to the absorbance from the a-Si:H and Ag constituents, respectively. The measured total absorbance A_{tot} of the Ag/a-Si:H nanocomposite and A_{ref} are also included.

detailed in Methods and Supporting Information. The presence of the Ag particles did not alter the measured dark conductivity significantly. This suggests that the Ag did not add much to the conduction in these samples, and that the nanoscale Schottky junctions[20] formed at the Ag/a-Si:H interfaces were not associated with a substantial depletion of free charge carriers in the a-Si:H films in the dark.

The photoconductance typically displayed a slow decrease over the course of a measurement, likely because of the photoinduced Staebler–Wronski degradation of a-Si:H.[21] To compensate for this effect as well as for any a-Si:H thickness variations of different samples, the photoconductance spectra were averaged over at least two samples and normalized by the value at 420 nm wavelength. Figure 2a–c shows the normalized photoconductance data averaged for samples of the same kind (either with or without Ag) for varying thickness. The reference photoconductance spectra follow the corresponding absorbance (see further below) quite closely. The latter is included in the same graphs for comparison.

In the context of light trapping structures for solar cells, the absorbance or photocurrent enhancement factor vis-à-vis a reference sample is conventionally used as a quantitative measure of the benefit.[22,23] In our measurements, the corresponding figure of merit is the photoconductivity enhancement factor $E = \langle\sigma\rangle/\langle\sigma_{ref}\rangle$, where $\langle\sigma\rangle$ is the averaged photoconductance spectrum for samples with Ag nanodisks and $\langle\sigma_{ref}\rangle$ is the corresponding spectrum for samples with the same thickness of a-Si:H but without the Ag nanodisks. This enhancement factor is shown in Figure 2d–f for the samples presented in Figure 2a–c, respectively. The enhancement factor exhibits a peak (somewhat noisy for the 12 nm film) located approximately at the plasmon resonance position of the Ag nanodisks. The peak value of the plasmon enhancement varies between 1.4 and 3.2 for the a-Si:H thicknesses studied in this work.

As a complement to the photoconductivity measurements, integrating sphere light absorbance measurements were carried out for a-Si:H films of varying thicknesses, with and without Ag nanodisks underneath. Examples are presented in Figure 2g–i. The a-Si:H absorption coefficient, and therefore the flat reference film absorbance, decreases monotonically with wavelength, as can also be observed in Figure 2g,h. For the thicker 67 nm film, Fabry–Perot interference results in a plateau in the range of 400–500 nm, as further detailed in Supporting Information. Compared to this flat film "reference absorption", the Ag/a-Si:H systems always display an enhanced response associated with the localized plasmon resonances of the Ag nanoparticles. It is not possible to calculate the fractions absorbed in the a-Si:H and Ag based on the absorbance data alone since the strong near-field coupling between these components will redistribute their isolated responses. To estimate the absorbance occurring in the a-Si:H part of the nanocomposite, we therefore exploit the measured photoconductivity enhancement data to obtain $A_{Si} \approx E \times A_{ref}$, where A_{ref} is the absorbance of the corresponding flat a-Si:H film. The basis for this estimate is the observed linearity between photoconductance and light absorption rate/photon flux. The result is plotted in Figure 2g–i. The absorbance of the Ag nanodisks A_{Ag} in the Ag/a-Si:H system may finally be obtained by use of the measured total absorbance, as $A_{Ag} = A_{tot} - A_{Si}$. As can be seen from Figure 2g–i, the plasmon resonance shifts with the a-Si:H thickness, for the studied system, from about 480 nm for the Ag nanodisks on glass (not shown) to about 600 and 680 nm for the same nanodisks covered with a 12 nm and a 32 nm a-Si:H films, respectively (Figure 2g,h). Such high sensitivity on the dielectric constant of the surrounding medium is well-known[24] and exploited, for instance, in sensing applications.[25] In the case of the 67 nm a-Si:H film, the higher order (quadrupolar) plasmon resonance mode becomes visible (see Figure 2i), an interpretation supported by the calculations discussed next.

Spatial Distribution, Thickness Dependence, and Mechanism of Enhancement. To clarify the nature of the observed plasmon-induced absorption and charge carrier generation, the experimental measurements were complemented by finite element calculations, as detailed in Methods and Supporting Information. The Helmholtz vector wave equation was solved for the scattered electric field, from which the total field within and around the plasmonic nanoparticles was obtained by superposition. This allowed us to calculate the total absorbance of the Ag/a-Si:H system and to resolve absorption occurring in the Ag and a-Si:H constituents, respectively. The results are compared with the measured data in Figures 3–5.

Figure 3 shows the measured and calculated total absorbance as a function of a-Si:H film thickness and photon wavelength. The calculations qualitatively reproduce the experimental results and allow for an interpretation of these observations. For a-Si:H thicknesses

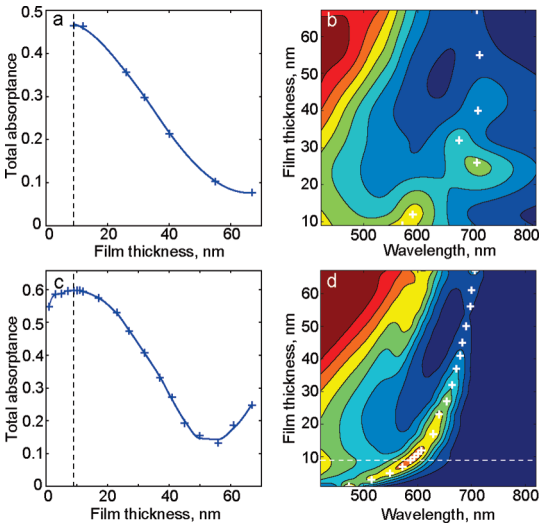

Figure 3. Experimental (a,b) and calculated (c,d) total absorbance of Ag/a-Si:H films. The data in (a) and (c) show the absorbance at the positions indicated by the crosses in (b) and (d), respectively. These locations correspond to maxima associated with the dipolar plasmon resonance for different film thicknesses. Interpolated curves were added as guides to the eye. The contour plots are smoothed surfaces approximating the data, with absorption ranging from high on the red side to low on the blue side of the color scale, respectively. The actual peak values are more accurately shown in (a) and (c). The minimum a-Si:H thickness studied experimentally is marked by dashed lines in (c) and (d).

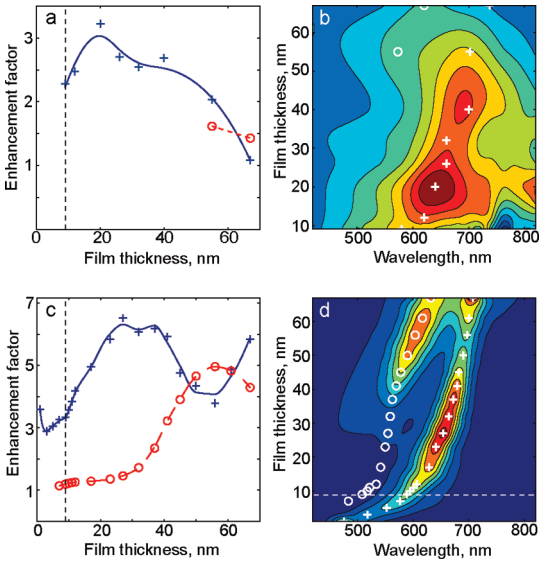

Figure 4. Experimental (a,b) and simulated (c,d) enhancement factors for a-Si:H films of different thicknesses. In (a) and (c), the values at local maxima for the enhancement factor are shown as a function of thickness. These maxima correspond to the positions marked in the contour plots (b) and (d), respectively; the maxima associated with the dipolar mode are marked by crosses, and the quadrupolar maxima are marked by circles. The contour plots are smoothed surfaces approximating the data.

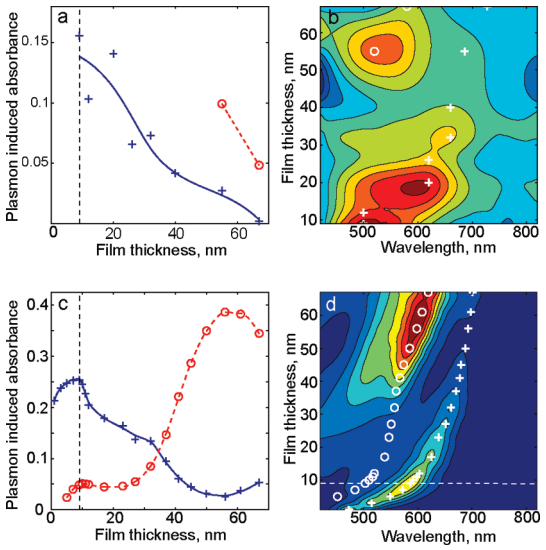

Figure 5. Plasmon-induced absorbance in the a-Si:H films from (a,b) experiments and (c,d) simulations. Crosses correspond to maxima of the dipolar part of ΔA, and circles represent maxima of the quadrupolar contribution. The contour plots are smoothed surfaces approximating the data.

of up to 40 nm, the mentioned shift of the Ag plasmon peak with a-Si:H thickness is clear in both the experiments and the simulations. This effect saturates somewhat for film thicknesses above 40 nm, at which point an additional absorption peak appears at shorter wavelengths. The field distribution associated with the latter has a quadrupolar character, as shown in Figure 1c, while the peak at longer wavelengths is mainly dipolar (see Figure 1b). The quadrupolar plasmon mode overlaps spectrally with strong absorption of the a-Si:H and is in the total absorbance only visible in the calculated data as a shoulder for the thickest films (at about 550−600 nm in Figure 3d). In the experimental data, the quadrupolar mode is however seen clearly in the Ag absorbance, for instance, for the 67 nm films of Figure 2i.

The appearance of the quadrupolar mode for thicker a-Si:H layers may qualitatively be understood since the high refractive index of the a-Si:H film (Figure S3 of Supporting Information) reduces the wavelength of light such that the Ag particle height becomes significant in comparison. Appreciable phase shifts occur from the top to the bottom of the absorbing layer and thereby stronger coupling to quadrupolar mode plasmon resonances.

While the total absorption of the quadrupolar mode increases with thickness up to some limit beyond the investigated range here, the experimental and simulated data show that the total absorbance associated with the dipolar mode has a maximum for very thin films (~10 nm) and that it thereafter mainly decreases with increasing a-Si:H thicknesses (Figure 3a,c). Such a maximum is suggested by theoretical considerations of the light absorption in close to two-dimensional nanocomposites, predicting further a maximum dipolar mode absorbance of 67% from the refractive index contrast between the glass and air in front and behind of the absorbing film, respectively.[18,26]

Although the experimental and calculated peak positions and thickness dependences agree well, peaks are both sharper and higher in the simulations. In the latter, the maximum dipolar absorbance (60%, Figure 3c) is in fact not very far from the theoretical maximum for this system, whereas the experimental maximum is somewhat lower (47%, Figure 3a). This relatively modest difference may have several origins, an obvious one being that the calculations were for a square array of particles, whereas the experiments were performed on significantly less ordered particle distributions (Figure 1e,g). This disorder creates varying environments of individual Ag nanoparticles and associated inhomogeneous peak broadening and lowering of the ensemble peak response.[27] Similar effects result from particle size and shape variations (Figure 1d,f). Although surface scattering was accounted for in the simulations, additional damping and broadening may exist in the experiments due to scattering at internal grain boundaries and by defects and impurities in the Ag disks. Differences in the coupling strength between the plasmonic disks and the a-Si:H layer (for instance, due to presence of oxide or other interfacial layers; see further Methods) could also have an influence. In light of these differences between the measured system and the simulated one, we regard the agreement between simulations and experiments to be quite good.

In Figure 4, experimental and calculated enhancement factors are compared. For film thicknesses up to about 30 nm, the dipolar peak dominates, while for thicker films, the quadrupolar mode gives rise to a ridge in the calculated contour map (Figure 4d) and a shoulder in the experimental map (Figure 4b). The positions of the enhancement peaks are well reproduced by the calculations, but the inhomogeneous peak broadening/lowering just mentioned above leads to peak amplitudes that are a factor 2−3 lower in the experimental data. For the thinnest films, part of this broadening may also be due to a lower signal-to-noise ratio.

The quadrupolar enhancement is visible only for the two thickest films in the experiments but fit the calculated trend for these points (Figure 4a,c).

The maximum dipolar enhancement observed in the experiments for the investigated range of a-Si:H thicknesses occurs for a thickness of 20 nm and agrees reasonably well with the calculated broad peak centered around 30 nm (Figure 4a,c). The value of the experimental dipolar enhancement factor decreases for thicker films, while the simulations, however, predict an increase for films thicker than 55 nm. Note, however, that the absorbance is very low under these conditions (see Figure 3d).

While the enhancement factor is the conventional way to represent light trapping benefits in solar cells,[22] it can be argued that the plasmon-induced absorbance in the a-Si:H films is a more interesting figure of merit for applicatons.[18] This is an absolute measure of the a-Si:H absorption caused by the Ag nanoparticles, defined as a difference $\Delta A \equiv A_{Si} - A_{ref}$ rather than as a ratio. Its dependence on thickness and wavelength is shown in Figure 5 and displays dipolar and quadrupolar ridges in both experiments and calculations.

Because of the strong increase of the a-Si:H absorbance toward shorter wavelengths, the maxima of ΔA associated with both dipolar and quadrupolar modes are shifted to somewhat shorter wavelengths and thinner a-Si:H films compared to the enhancement factor maxima. The overall effect is a stronger peak absorbance in the a-Si:H in absolute terms. The experimental ΔA peaks are in addition blue-shifted compared to the calculated peaks, which we believe is a secondary effect of their broader spectral range and the increasing a-Si:H absorption coefficient toward the blue (Figure S3 of Supporting Information). The experimental dipolar peak dependence on film thickness demonstrates a maximum for the thinnest, 9 nm a-Si:H film, and a mainly declining trend with thickness (Figure 5a). The extended calculated response (Figure 5c) indeed confirms a maximum at 9 nm thickness and displays an initially sharp decline of ΔA with increasing thickness. The maximum observed for these very thin films is closely related to the maximum of the total absorbance (Figure 2a,c), which in turn can be understood from the general properties of this virtually two-dimensional system.[26] It is a near-field dominated effect, with the FEM calculated absorption concentrated to the vicinity of the Ag nanoparticles; a far-field enhancement by means of waveguided modes[23] is not possible here, as the fundamental mode is cut off for an a-Si:H thickness of 35 nm at the peak wavelength of about 580 nm.[28] We note that the calculated dependence of the dipolar ΔA peak shows a knee-like decline near 30 nm a-Si:H thickness, which appears to be connected to the onset of the quadrupolar mode.

The quadrupolar mode observed in the calculation of the a-Si:H absorption for the thinner films (<50 nm) was weak and not clearly resolved in the experiments. Additional simulations (not shown here) suggest that the effect of the quadrupolar mode on the a-Si:H absorbance is quite sensitive to the a-Si:H coverage on top of the particles, which is in line with previous results demonstrating the predominant localization of this mode toward the "air" side of the structure[29] (see also Figure 1c). The quite substantial difference in peak values of the experimental and calculated quadrupolar ΔA may therefore be due to deviations in how the a-Si:H cover the particles from the way it was assumed in the simulations (see Methods). Compared to dipolar resonances, the spatially less extended near-field of quadrupolar resonances outside the particles may also imply a more significant rate of charge carrier recombination at the metal/semiconductor interface, which is not taken into account in the calculations.

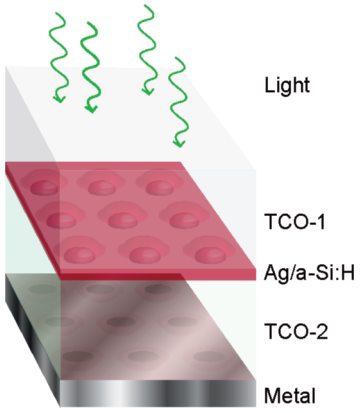

Figure 6. Photovoltaic configuration where the broad-band plasmon near-field induced absorption in an a-Si:H coated array of Ag nanoparticles can be maximized. The a-Si:H layer is about 20 nm thick, and the spacer layer (TCO-2) is around 100 nm. The metallic back reflector also serves as an electrode.

Calculations were extended into the range from 1 to 9 nm, the latter being the thinnest film studied experimentally. The total absorbance remains high over this range due to internal dissipation in the Ag, while for the thinnest films, the enhancement factor actually starts to increase again; it diverges in the limit of zero thickness, as was previously observed.[15] In contrast, the plasmon-induced absorbance in the a-Si:H layer decreases to zero in this limit, although in remarkably slow fashion owing to the exceptionally high damping of a-Si:H for short wavelengths (<500 nm).

The envisioned implementation of these plasmonic nanocomposites in solar cells requires a dedicated device architecture to be developed. Given a total absorber layer thickness around 10−20 nm, p-n- and p-i-n-type homojunctions are unlikely to sustain a sufficiently sharp potential drop for efficient charge separation, leaving heterojunctions or metal/semiconductor-type junctions as the preferred option. To allow for the most optically efficient design with a reflective support,[6] transparent conducting oxides (TCOs) or their equivalents are further required for contacting the absorber layer on both the front- and backside. Thus in the simplest case, the TCO-1/[Ag/a-Si:H]/TCO-2/metal configuration shown in Figure 6 is envisaged, where the two TCOs must be carefully chosen for optimal driving force (work function difference),[30] band edge alignments, and conductivity/transparency trade-offs. Since the charge carriers will be generated in close proximity to the metal nanoparticles, the latter may beneficially be integrated with the circuit rather than isolated. An intelligent use of very thin selective ohmic contacts[31] is an option to reduce recombination *via* the noble metal surfaces and to improve charge separation further. The

growth of ultrathin (~1 nm), pinhole-free selective barrier films for this purpose is one of the many challenges requiring further investigation. In light of the unique opportunities that these systems provide in terms of resource efficiency and cost reductions, such a prospect nevertheless appears worthwhile.

CONCLUSIONS

We have investigated the plasmon near-field induced light absorption in a-Si:H films and its dependence on film thickness, by means of optical and photoconductivity measurements and numerical calculations. The linear response of the measured photoconductivity allows for a straightforward quantification of the useful charge carrier generation rate when combined with optical spectroscopy.

Numerical calculations by FEM match the experimental results well and allow different features to be associated with plasmon resonances of predominantly dipolar and quadrupolar character. The wavelength positions and thickness dependences of the plasmon enhancement peaks are well reproduced, while there is less agreement for peak widths and absolute amplitudes. The latter is understood tentatively in terms of inhomogeneous broadening due to individual variations of the experimental Ag particle geometries (sizes, shapes, and microstructure) and their varying coupling with the a-Si:H layer as well as with neighboring particles.

We evaluated the photoconductivity response in terms of different figures of merit: the peak plasmon-induced a-Si:H absorbance and the more commonly used absorption enhancement factor. These different evaluation criteria are shown to lead to different optima for the a-Si:H thickness; the plasmon-induced absorbance is maximized close to a local maximum for the total absorbance, whereas the enhancement factor favors thicker a-Si:H films with lower absolute rate of useful charge carrier generation.

The results of our combined experimental and numerical study show promise for the development of ultrathin (~10 nm) "two-dimensional" plasmonic solar cells, with up to 15% plasmon-induced absorbance measured in a-Si:H films as thin as 9 nm for a wavelength close to the plasmon peak position. The plasmon contribution increases the a-Si:H absorbance from 22 to 37% at this optimum. We anticipate that, with increased control of the geometry to reduce inhomogeneous effects, the maximum plasmon-induced absorbance (25% at the plasmon peak wavelength) calculated for the same thickness may be approached. Additional optimization of the geometrical parameters, in particular, the particle volumes and separations, will further help approach the theoretical limit for absorption in two-dimensional systems. If the latter optimization is performed with a spacer and reflector added behind the nanocomposite absorber layer, the theoretical peak absorbance approaches 100%, making it feasible to bring the useful wavelength integrated absorption of this system to levels of high interest for real solar cell applications. A photovoltaic configuration devoted to such purposes was briefly discussed.

METHODS

The model system employed in this work comprises Ag nanodisks of diameter 60 nm and height 40 nm, nominally, covered with an a-Si:H film of thickness between 9 and 67 nm. As a reference system, a flat a-Si:H film without the nanoparticles was used. The Ag nanodisks were fabricated by hole-mask colloidal lithography (see further Supporting Information),[32] which provides nanodisks with a rather uniform size distribution (up to 10% dispersion;[32] see Figure 1d) quasi-randomly positioned on the surface with a coverage of about 6% (Figure 1b,c). The a-Si:H films were deposited on top of the nanodisks and on bare glass for reference using plasma-enhanced chemical vapor deposition (PECVD). The deposition recipe differed from the classical recipe of "device quality" a-Si:H films for solar cells[33] in that the substrate was not heated during the deposition; instead, the chip was post-annealed at 200 °C in H_2/Ar atmosphere (see Supporting Information for details). Spectroscopic ellipsometry was used to obtain the optical constants and thicknesses of the a-Si:H films to use in the simulations. The optical constants and dark conductivities of our films were found to be close to the literature values for standard a-Si:H films.

Photoconductivity measurements were combined with measurements of the light absorption to deduce the nanoparticle plasmon-induced absorption in the a-Si:H films (see Supporting Information). The photoconductivity was measured on chips with lithographically fabricated electrode patterns, on which the Ag nanodisks and a-Si:H films were deposited. Light absorbance was deduced from integrating sphere measurements on a-Si:H and Ag/a-Si:H samples equivalent to those used for the photoconductivity measurements.

The system was numerically simulated by solving the Helmholtz equation for the scattered electric field, using Comsol Multiphysics and procedures previously outlined in detail.[29] The quasi-random Ag distribution (Figure 1) was represented as a periodic square array, with all nanoparticles having the same size and shape (see Supporting Information). The particles had the nominal dimensions and average spacing of the experiments. A slight cone shape was assumed (16° half angle[32]), and the edges were rounded with a 2.2 nm radii to match the plasmon resonance for the uncoated Ag particles. Presence of native oxide and/or organic contamination on the surface of the Ag nanoparticles was quite likely, as the samples were exposed to air between depositions. Such layers spatially separate the a-Si:H coating from the Ag nanodisks slightly, leading to a reduced near-field intensity in the a-Si:H. A 3 nm spacer with a real refractive index of 1.5 was assumed to represent this situation in an effective sense in the calculations, which resulted in a fair agreement with the observed dipolar peak position as a function of a-Si:H thickness.

Acknowledgment. The authors thank Ö. Arthursson and C. Wadell for the SEM images, T. Wagner for help with analysis of the ellipsometry data, and C. Langhammer for assistance with the integrating sphere measurements. The Swedish Energy Agency, contract 0189-1, *Nanoscience and Nanotechnology for Sustainable Energy and Environment (NANO-SEE)*, is gratefully acknowledged for the financial support.

Supporting Information Available: Description of the experimental procedures and calculations, optical characterization of the a-Si:H films. This material is available free of charge *via* the Internet at http://pubs.acs.org.

REFERENCES AND NOTES

1. Green, M. A.; Emery, K.; Hishikawa, Y.; Warta, W. Solar Cell Efficiency Tables (Version 34). *Prog. Photovoltaics* **2009**, *17*, 320–326.
2. Shockley, W.; Queisser, H. J. Detailed Balance Limit of Efficiency of p-n Junction Solar Cells. *J. Appl. Phys.* **1961**, *32*, 510–519.
3. Araujo, G. L.; Marti, A. Absolute Limiting Efficiencies for Photovoltaic Energy-Conversion. *Sol. Energy Mater. Sol. Cells* **1994**, *33*, 213–240.
4. Rech, B.; Wagner, H. Potential of Amorphous Silicon for Solar Cells. *Appl. Phys. A: Mater. Sci. Process.* **1999**, *69*, 155–167.
5. Shah, A.; Meier, J.; Buechel, A.; Kroll, U.; Steinhauser, J.; Meillaud, F.; Schade, H.; Domine, D. Towards Very Low-Cost Mass Production of Thin-Film Silicon Photovoltaic (PV) Solar Modules on Glass. *Thin Solid Films* **2006**, *502*, 292–299.
6. Hägglund, C.; Apell, S. P. Resource Efficient Plasmon-Based 2D-Photovoltaics with Reflective Support. *Opt. Express* **2010**, *18*, A343–A356.
7. Naughton, M. J.; Kempa, K.; Ren, Z. F.; Gao, Y.; Rybczynski, J.; Argenti, N.; Gao, W.; Wang, Y.; Peng, Y.; Naughton, J. R.; *et al.* Efficient Nanocoax-Based Solar Cells. *Phys. Status Solidi RRL* **2010**, *4*, 181–183.
8. McFarland, E. W.; Tang, J. A Photovoltaic Device Structure Based on Internal Electron Emission. *Nature* **2003**, *421*, 616–618.
9. Kempa, K.; Naughton, M. J.; Ren, Z. F.; Herczynski, A.; Kirkpatrick, T.; Rybczynski, J.; Gao, Y. Hot Electron Effect in Nanoscopically Thin Photovoltaic Junctions. *Appl. Phys. Lett.* **2009**, *95*, 233121.
10. Moulin, E.; Luo, P. Q.; Pieters, B.; Sukmanowski, J.; Kirchhoff, J.; Reetz, W.; Muller, T.; Carius, R.; Royer, F. X.; Stiebig, H. Photoresponse Enhancement in the Near Infrared Wavelength Range of Ultrathin Amorphous Silicon Photosensitive Devices by Integration of Silver Nanoparticles. *Appl. Phys. Lett.* **2009**, *95*, 033505.
11. Ferry, V. E.; Verschuuren, M. A.; Li, H. B. T.; Verhagen, E.; Walters, R. J.; Schropp, R. E. I.; Atwater, H. A.; Polman, A. Light Trapping in Ultrathin Plasmonic Solar Cells. *Opt. Express* **2010**, *18*, A237–A245.
12. Zhu, J.; Hsu, C.-M.; Yu, Z.; Fan, S.; Cui, Y. Nanodome Solar Cells with Efficient Light Management and Self-Cleaning. *Nano Lett.* **2010**, *10*, 1979–1984.
13. Derkacs, D.; Lim, S. H.; Matheu, P.; Mar, W.; Yu, E. T. Improved Performance of Amorphous Silicon Solar Cells *via* Scattering from Surface Plasmon Polaritons in Nearby Metallic Nanoparticles. *Appl. Phys. Lett.* **2006**, *89*, 093103.
14. Ferry, V. E.; Verschuuren, M. A.; Li, H. B. T.; Schropp, R. E. I.; Atwater, H. A.; Polman, A. Improved Red-Response in Thin Film a-Si:H Solar Cells with Soft-Imprinted Plasmonic Back Reflectors. *Appl. Phys. Lett.* **2009**, *95*, 183503-3.
15. Rockstuhl, C.; Lederer, F. Photon Management by Metallic Nanodiscs in Thin Film Solar Cells. *Appl. Phys. Lett.* **2009**, *94*, 213102.
16. Tsai, F.-J.; Wang, J.-Y.; Huang, J.-J.; Kiang, Y.-W.; Yang, C. C. Absorption Enhancement of an Amorphous Si Solar Cell through Surface Plasmon-Induced Scattering with Metal Nanoparticles. *Opt. Express* **2010**, *18*, A207–A220.
17. Wang, F.; Shen, Y. R. General Properties of Local Plasmons in Metal Nanostructures. *Phys. Rev. Lett.* **2006**, *97*, 206806.
18. Hägglund, C.; Kasemo, B. Nanoparticle Plasmonics for 2D-Photovoltaics: Mechanisms, Optimization, and Limits. *Opt. Express* **2009**, *17*, 11944–11957.
19. Standridge, S. D.; Schatz, G. C.; Hupp, J. T. Distance Dependence of Plasmon-Enhanced Photocurrent in Dye-Sensitized Solar Cells. *J. Am. Chem. Soc.* **2009**, *131*, 8407–8409.
20. Hägglund, C.; Zhdanov, V. P. Charge Distribution on and near Schottky Nanocontacts. *Phys. E* **2006**, *33*, 296–302.
21. Tatsuo, S. Staebler–Wronski Effect in Hydrogenated Amorphous Silicon and Related Alloy Films. *Jpn. J. Appl. Phys.* **2004**, *43*, 3257–3268.
22. Yablonovitch, E.; Cody, G. D. Intensity Enhancement in Textured Optical Sheets for Solar-Cells. *IEEE Trans. Electron Devices* **1982**, *29*, 300–305.
23. Stuart, H. R.; Hall, D. G. Absorption Enhancement in Silicon-on-Insulator Waveguides Using Metal Island Films. *Appl. Phys. Lett.* **1996**, *69*, 2327–2329.
24. Kelly, K. L.; Coronado, E.; Zhao, L. L.; Schatz, G. C. The Optical Properties of Metal Nanoparticles: The Influence of Size, Shape, and Dielectric Environment. *J. Phys. Chem. B* **2003**, *107*, 668–677.
25. Larsson, E. M.; Langhammer, C.; Zorić, I.; Kasemo, B. Nanoplasmonic Probes of Catalytic Reactions. *Science* **2009**, *326*, 1091–1094.
26. Hägglund, C.; Apell, S. P.; Kasemo, B. Maximized Optical Absorption in Ultrathin Films and Its Application to Plasmon-Based Two-Dimensional Photovoltaics. *Nano Lett.* **2010**, *10*, 3135–3141.
27. Persson, B. N. J.; Liebsch, A. Optical-Properties of Two-Dimensional Systems of Randomly Distributed Particles. *Phys. Rev. B* **1983**, *28*, 4247–4254.
28. Tien, P. K. Light Waves in Thin Films and Integrated Optics. *Appl. Opt.* **1971**, *10*, 2395–2413.
29. Hägglund, C.; Zäch, M.; Petersson, G.; Kasemo, B. Electromagnetic Coupling of Light into a Silicon Solar Cell by Nanodisk Plasmons. *Appl. Phys. Lett.* **2008**, *92*, 053110.
30. Centurioni, E.; Iencinella, D. Role of Front Contact Work Function on Amorphous Silicon/Crystalline Silicon Heterojunction Solar Cell Performance. *IEEE Electron Device Lett.* **2003**, *24*, 177–179.
31. Fonash, S. J. *Solar Cell Device Physics*, 2nd ed.; Academic Press: Burlington, MA, 2010; p 353.
32. Fredriksson, H.; Alaverdyan, Y.; Dmitriev, A.; Langhammer, C.; Sutherland, D. S.; Zäch, M.; Kasemo, B. Hole-Mask Colloidal Lithography. *Adv. Mater.* **2007**, *19*, 4297–4302.
33. Schropp, R. E. I.; Zeman, M. *Amorphous and Microcrystalline Silicon Solar Cells: Modeling, Materials and Device Technology*; Kluwer Academic Publishers: Boston/Dordrecht/London, 1998; p 207.